Comparing Optical Oscillators across the Air to Milliradians in Phase and 10^{-17} in Frequency

Laura C. Sinclair,[1] Hugo Bergeron,[2] William C. Swann,[1] Esther Baumann,[1]
Jean-Daniel Deschênes,[2] and Nathan R. Newbury[1]

[1]*National Institute of Standards and Technology, 325 Broadway, Boulder, Colorado 80305, USA*
[2]*Université Laval, 2325 Rue de l'Université, Québec, QC G1V 0A6, Canada*

We demonstrate carrier-phase optical two-way time-frequency transfer (carrier-phase OTWTFT) through the two-way exchange of frequency comb pulses. Carrier-phase OTWTFT achieves frequency comparisons with a residual instability of 1.2×10^{-17} at 1 s across a turbulent 4-km free space link, surpassing previous OTWTFT by 10–20 times and enabling future high-precision optical clock networks. Furthermore, by exploiting the carrier phase, this approach is able to continuously track changes in the relative optical phase of distant optical oscillators to 9 mrad (7 as) at 1 s averaging, effectively extending optical phase coherence over a broad spatial network for applications such as correlated spectroscopy between distant atomic clocks.

Applications of future optical clock networks include time dissemination, chronometric geodesy, coherent sensing, tests of relativity, and searches for dark matter among others [1–14]. This promise has motivated continued advances in optical clocks and oscillators [15–19] and in the optical transfer techniques to network them. In particular, time-frequency transfer over fiber-optic networks has seen tremendous progress [1,7,20–23]. However, many applications require clock networks connected via free-space links. Direct adoption of fiber-based approaches to free space is possible but hampered by atmospheric turbulence [24]. Satellite-laser-ranging approaches such as time transfer by laser link (T2L2) are being actively explored [25–28]. Here, we consider optical two-way time-frequency transfer (OTWTFT) based on the two-way exchange of frequency comb pulses [24,29–35]. This approach exploits the reciprocity (equality) in the time of flight for light to travel in each direction across a single-mode link [36], just as in rf-based two-way satellite time-frequency transfer [37–39] and analogous fiber-optic demonstrations [23,40–42]. In previous work, this OTWTFT approach used the arrival time of the frequency comb pulses to support frequency comparisons at residual instabilities of $\sim 4 \times 10^{-16}$ at 1-s averaging times [29], and ultimately to enable subfemtosecond time synchronization of distant optical and microwave-based clocks [32–34].

Here, we demonstrate OTWTFT can exploit the carrier phase of the frequency comb pulses for much higher performance. While carrier-phase measurements are relatively straightforward across optical fiber because of the uninterrupted stable signal, the same is not true of a free-space link where atmospheric turbulence leads to strong phase noise and signal intermittency, in turn presenting a severe challenge to "unwrapping" the measured phase

without catastrophic $\pm \pi$ phase errors. We show such phase unwrapping is possible over hour durations, despite atmospheric turbulence, and despite strong phase drift between the distant sites. We achieve frequency comparison with a residual instability (modified Allan deviation) of 1.2×10^{-17} at 1 s: 10–20 times lower than achieved with the pulse timing alone. This instability drops to 6×10^{-20} at 850 s. We show the short-term residual instability is near the limit given by atmospheric-turbulence-driven reciprocity breakdown. Most importantly, it is well below the absolute instability of even the best optical clocks and oscillators.

Carrier-phase OTWTFT essentially tracks the evolution of the relative optical phase between the two distant optical oscillators. Specifically, here we track the ~ 300 million-radian residual phase evolution between our two 1535-nm cavity-stabilized lasers without ambiguity to within a 0.2-rad standard deviation at 400-μs time resolution. The corresponding time deviation reaches 7 as (9 mrad) at 1-s averaging time. The relative phase noise power spectral density drops below 10^{-4} rad^2/Hz (~ 60 as^2/Hz) at 1 Hz offset, or >25 dB below that achievable with pulse timing alone. In this sense, we establish tight mutual optical phase coherence between sites that could be exploited in future applications requiring spatially distributed phase coherence. In particular, several groups have compared optical atomic clocks to ultra-high precision by canceling out common-mode optical phase noise of the clocks' local oscillators. Takamoto *et al.* demonstrated synchronous sampling of two distant atomic ensembles, avoiding the Dick effect [43], while Chou *et al.* and others demonstrated correlated spectroscopy to extend the Ramsey interrogation times beyond the local oscillator coherence time [44–46]. Carrier-phase OTWTFT could enable such distant optically coherent measurements even with

portable (but noiser) cavity-stabilized lasers [47–50] and even over turbulent links.

To successfully track the optical phase, the interval between phase measurements must be shorter than the mutual phase coherence time between the distant optical oscillators. (For the same reason an optical clock's Ramsey interrogation time is limited by the local oscillator coherence time.) Otherwise, the resulting $\pm\pi$ phase ambiguities lead to complete loss of frequency and phase information. This presents two problems for carrier-phase OTWTFT over a turbulent atmosphere. First, atmospheric turbulence scrambles the received light's optical phase, degrading the mutual optical coherence time. This problem is circumvented by exploiting the time-of-flight reciprocity. Second, atmospheric turbulence causes fades (signal loss) at random times, with random durations and random separations, so the measurement interval often exceeds the mutual coherence time (of 50 ms here). This problem is circumvented by combining the timing information from both the pulse's carrier phase and envelope to extend the coherence across the fades.

We use a folded 4-km link (Fig. 1) to compare optical oscillators at site A and B. At each site, a cavity-stabilized laser serves as the optical oscillator. We let the oscillator at site A define the time scale with known frequency ν_A and phase $\varphi_A(t) = 2\pi\nu_A t$. The optical phase of site B's oscillator is $\varphi_B(t) = 2\pi\nu_B t + \delta\varphi(t)$, where the first term is the phase evolution from the *a priori* estimated frequency $\nu_B \neq \nu_A$
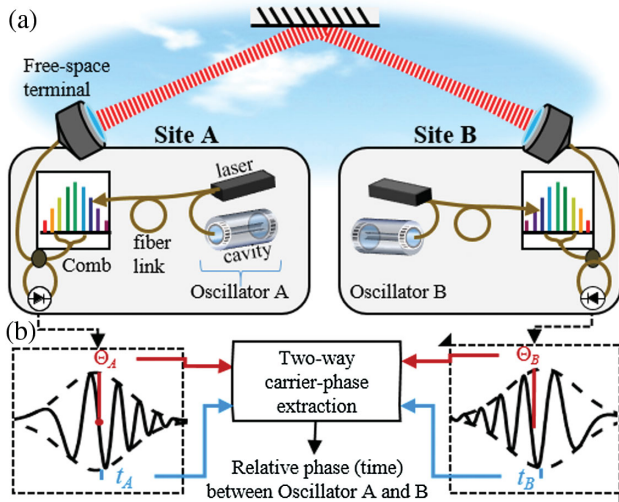
FIG. 1. (a) Experimental setup. The phase of the local optical oscillator (cavity-stabilized laser) is transferred via a Doppler-canceled fiber link to a frequency comb, a portion of whose output is transmitted to the opposite site, where it is heterodyned against the local comb. The link is folded, i.e., A and B are physically adjacent, to permit acquisition of truth data. (b) The resulting cross-correlation between pulse trains is analyzed to extract the envelope peak time, $t_{p,X}$, and the phase, $\Theta_{p,X}$, which are input to a Kalman-filter based algorithm to calculate the relative phase or timing evolution between the two optical oscillators despite atmospheric phase noise and fading.

and the second captures the unknown phase wander or equivalently timing wander $\delta\tau = (2\pi\nu_B)^{-1}\delta\varphi$. The unknown frequency variation is $\delta\nu(t) = (2\pi)^{-1}d\delta\varphi(t)/dt$. Our objective is to measure $\delta\varphi(t)$ or, equivalently, $\delta\nu(t)$. We drop any constant phase offset by setting $\delta\varphi(0) = 0$ [and so $\delta\tau(0) = 0$] since its knowledge requires full time synchronization. The folded link permits truth data acquisition via a direct optical heterodyne measurement, which also necessitates both oscillators operate at nearly the same frequency, here at $\nu_A = 194.584\,000$ and $\nu_B = 194.584\,197$ THz. In general, however, the optical oscillators would be at widely different frequencies and locations. Additional details on the combs and free-space terminals are in Refs. [32,51] with additional experimental values given in the Supplemental Material, Table 1 [52].

At each site, the optical oscillator signal is transferred via a Doppler-canceled fiber link to a self-referenced frequency comb where its phase is mapped onto the comb. Specifically, at site B the relative phase noise $\delta\varphi(t)$ maps to noise in both the optical phase and the timing of comb B's pulse train. This noise is not white but includes strong random frequency walk. We compare the phase and timing of comb B with comb A via linear optical sampling in a two-way configuration. To do this, combs A and B are phase locked using our *a priori* information of ν_A and ν_B such that their repetition frequencies $f_{r,A}$ and $f_{r,B}$ differ by $\Delta f_r = f_{r,B} - f_{r,A}$. Here, $f_{r,A} = 200$ MHz with $\Delta f_r \approx 2.46$ kHz. At each site, we filter the comb to a $\sim$1-THz bandwidth around 1560 nm and transmit it to the opposite site where it is heterodyned against the local comb to generate a series of cross-correlations, which are analyzed to extract $\delta\varphi(t)$. Note the transmitted comb optical spectrum need not—and does not—encompass the optical oscillator frequencies.

The extraction of $\delta\varphi(t)$ proceeds as follows. For convenience, we lock the self-referenced combs such that $f_{r,A} = \nu_A/n_A$ and $f_{r,B} = \nu_B/n_B$, where n_A and n_B are the indices of the comb tooth nearest to the local oscillator at sites A and B. We then identify the pair of comb tooth frequencies, $\tilde{\nu}_A$ and $\tilde{\nu}_B$, nearest to the center of the transmitted optical spectrum having a frequency separation $\Delta\tilde{\nu} \equiv \tilde{\nu}_B - \tilde{\nu}_A < \pm\Delta f_r/2$. This pair, rather than ν_A and ν_B directly, will serve as the carrier frequencies for the carrier-phase OTWTFT, as shown below. At site A, we write the transmitted and received comb electric fields with respect to this pair as

$$E_A(t) = e^{i2\pi\tilde{\nu}_A t}\sum_m E_{A,m}e^{i2\pi m f_{r,A}t},$$

$$E_B(t) = e^{i2\pi\tilde{\nu}_B(t-T_{\text{link}})}e^{i\tilde{\nu}_B\delta\varphi/\nu_B}\sum_m E_{B,m}e^{i2\pi m f_{r,B}(t+\delta\tau-T_{\text{link}})},$$

$$(1)$$

where $E_{X,m}$ is the electric field, m is the comb index from the tooth at $\tilde{\nu}_X$, T_{link} is the slowly varying time of flight, and $\delta\tau = (2\pi\nu_B)^{-1}\delta\varphi$ is the timing jitter of comb B. The equations for site B are analogous, except that T_{link} appears

in $E_A(t)$. Note the unknown phase wander of oscillator B appears both in the timing noise $\delta\tau$ and in the carrier optical phase of comb B. At each site, the combs are heterodyned to give a series of cross-correlations with complex envelopes $I_X(t)$, labeled by the integer p

$$V_X(t) \propto e^{i\Theta_{p,X}} \sum_p I_X(t - t_{p,X}), \qquad (2)$$

assuming T_{link} and $\delta\tau$ vary slowly on the time scales of $1/\Delta f_r$. (See Supplemental Material [52] for derivation.) The cross-correlation envelope peaks at times

$$t_{p,A} = \Delta f_r^{-1}\{p + f_{r,B}T_{\text{link}} - f_{r,B}\delta\tau\},$$
$$t_{p,B} = \Delta f_r^{-1}\{p - f_{r,A}T_{\text{link}} - f_{r,B}\delta\tau\}, \qquad (3)$$

with phase

$$\Theta_{p,A} = 2\pi\Delta\tilde{\nu}t_{p,A} - 2\pi\tilde{\nu}_B T_{\text{link}} + \tilde{\nu}_B\nu_B^{-1}\delta\varphi,$$
$$\Theta_{p,B} = 2\pi\Delta\tilde{\nu}t_{p,B} + 2\pi\tilde{\nu}_A T_{\text{link}} + \tilde{\nu}_B\nu_B^{-1}\delta\varphi. \qquad (4)$$

As expected for a two-way measurement, the time of flight enters with an opposite sign at the two sites in Eqs. (3) and (4) and can thus be eliminated. Note the cross-correlations do not occur simultaneously at the two sites, rather asynchronously with offset $|t_{p,A} - t_{p,B}| < 2/\Delta f_r$, which will be important later. For each site, we evaluate $t_{p,X}$ and $\Theta_{p,X}$ at $1/\Delta f_r \sim 400 \ \mu$s intervals via matched filter processing against the $p = 0$ cross-correlation, thereby dropping any overall constant time or phase offsets.

In previous OTWTFT, we effectively solved Eq. (3) for $\delta\tau(t_p)$ evaluated at $t_p \equiv (t_{p,A} + t_{p,B})/2$, from which we extracted the fractional frequency uncertainty $\delta\nu/\nu_B = d\delta\tau/dt$. However, the precision of $\delta\tau(t_p)$ is typically SNR limited to 3 to 8 fs (4 to 10 rad equivalent optical-phase uncertainty).

In carrier-phase OTWTFT, we exploit the cross-correlation phase for higher precision by solving Eq. (4) to find

$$\delta\varphi(t_p) \approx \frac{\nu_B}{2\tilde{\nu}_B}\{\Theta_{p,A} + \Theta_{p,B} - 4\pi\Delta\tilde{\nu}t_p + 2\pi\Delta\tilde{\nu}T_{\text{link}} - 2\pi k_p\},$$

$$(5)$$

dropping the next term $\pi\nu_B(t_{p,A} - t_{p,B})dT_{\text{link}}/dt$. (See Supplemental Material [52].) After determining T_{link} from Eq. (3), all the terms are known except for k_p, which is a time-dependent integer accounting for the π ambiguity (~ 2.5 fs equivalent timing uncertainty) in this phase measurement. The precision is now limited by the ~ 0.1 rad noise typical of the comb phase locks and Doppler-canceled links for a total uncertainty of ~ 0.2 rad, corresponding to 160 as in timing precision at the 400-μs update rate.

Of course, this higher precision is lost in π ambiguities unless k_p is known. If $\delta\varphi$ varies slowly with successive measurements, standard unwrapping algorithms can track k_p. However, $\delta\varphi$ varies significantly from mutual phase noise

between the oscillators, characterized by the measured power spectral density (PSD) of $S_{\delta\varphi} = 22f^{-4} \ \text{rad}^2/\text{Hz}$, where f is the Fourier frequency. More importantly, random fades from turbulence-induced scintillation, physical obstructions, or loss of terminal pointing cause measurement gaps well beyond $1/\Delta f_r \sim 400 \ \mu$s. Therefore, a layered Kalman-filter-based unwrapping algorithm is used. (See Supplemental Material [52].) The inputs are the first four terms of Eq. (5), $S_{\delta\varphi}$, $\delta\tau(t_p)$ from Eq. (3), the received power, and the power-dependent uncertainty in $t_{p,X}$ and $\Theta_{p,X}$. The output is a prediction of the phase, which is compared with the observed phase to find k_p. The Kalman filter also predicts the uncertainty $\sigma_{\varphi,p}$ in the predicted phase which grows with time over long fades, eventually leading to ambiguity in k_p and requiring use of the envelope timing to re-acquire k_p. Indeed, a functional, rigorous definition of mutual coherence time is exactly the time interval until the predicted phase's uncertainty exceeds a value σ_φ, denoted $t_{\text{coh}}^{\sigma_\varphi}$. (This coherence time differs from frequency-domain definitions based on linewidth or PSDs which are poorly defined for $S_{\delta\varphi} \propto f^{-4}$, and is in fact closely related to the relevant coherence for Ramsey interrogation [19]). For our system, $t_{\text{coh}}^{1 \text{ rad}} \sim 50$ ms. However, the algorithm uses a stricter limit of $t_{\text{coh}}^{0.12 \text{ rad}} \sim 7$ ms before reverting to the envelope timing to "re-acquire" k_p. While all processing is currently offline, real-time processing following Ref. [32] is possible.

Figure 2(a) shows the resulting unwrapped phase $\delta\varphi(t)$ over a ~ 1.4-h measurement across the 4-km turbulent link. It is dominated by a roughly linear frequency drift, leading to over 300×10^6 rad of total phase drift [beyond the expected phase drift of $2\pi(\nu_B - \nu_A)t$] with random phase wander reflecting the f^{-4} PSD, as shown in the inset. Therefore, phase continuity of the measured $\delta\varphi(t)$ can only be evaluated by comparison with truth data, $\delta\varphi_{\text{truth}}(t)$, acquired from the direct shorted heterodyne beat between oscillators. As shown in Fig. 2(b), $\delta\varphi(t) - \delta\varphi_{\text{truth}}(t)$ shows no phase slips. The standard deviation is 0.2 rad (or 160 as in time units) at the full 400-μs sample rate and 30 mrad (24 as) at a 1-s time resolution. Finally, a linear fit to $\delta\varphi(t) - \delta\varphi_{\text{truth}}(t)$ yields the overall accuracy in the determination of oscillator B's frequency offset $\delta\nu$ across the measurement, which is $2 \pm 20 \ \mu$Hz.

Although it is not evident in the densely plotted data of Figs. 2(a) and 2(b), fades occur during 1% of the total 1.4 h. Because of turbulence, for ~ 3 mW transmitted power, the received power varied from 0 to 5 μW with a detection threshold of 10 nW, below which a fade (signal loss) occurs. Fades with durations beyond $t_{\text{coh}}^{0.12 \text{ rad}} \sim 7$ ms require re-acquisition of the phase via the envelope. Figures 2(c) and (d) show examples of phase-continuous measurement across a single fade and across multiple juxtaposed fades. For the data of Fig. 2(b), there are ~ 1400 fades randomly distributed in time with durations beyond $t_{\text{coh}}^{0.12 \text{ rad}} \sim 7$ ms, while a later run had 26% fades with $\sim 28\,500$ fades beyond $t_{\text{coh}}^{0.12 \text{ rad}}$ (see Supplemental Material [52], Fig. 1).
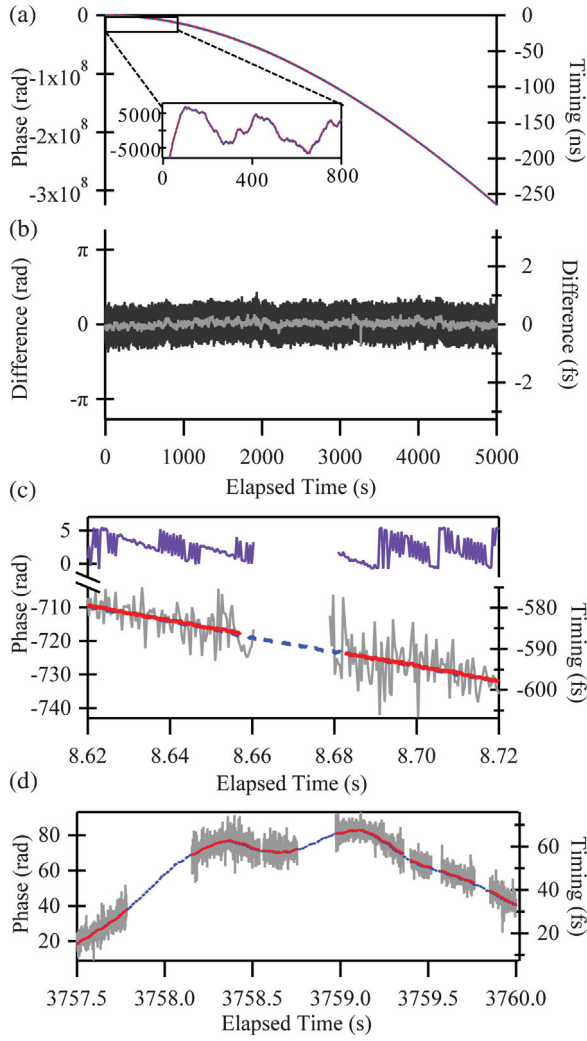
FIG. 2. Results for ~1.4 h across the turbulent 4-km link. (a) Oscillator B's residual phase from carrier-phase OTWTFT, $\delta\varphi(t)$, (red line) and from direct oscillator-to-oscillator truth data, $\delta\varphi_{\text{truth}}(t)$, (dashed blue line) in radians (left axis) and scaled to time units by $(2\pi\nu_B)^{-1}$ (right axis). The dominant quadratic behavior arises from the ~4 Hz/s frequency drift between the optical oscillators. Inset: phase wander after removing a quadratic fit illustrating the phase fluctuations at all time scales expected from the $1/f^4$ relative phase noise. (b) Difference between the carrier-phase OTWTFT and truth data, $\delta\varphi(t) - \delta\varphi_{\text{truth}}(t)$, at 400 μ sec sampling (black) with 0.2 rad (160 as) standard deviation and at 1-s averaging (gray) with 30 mrad (24 as) standard deviation. There are no phase discontinuities over the entire period. (c) A 10-s segment showing the phase before unwrapping (top panel, purple) and after (red line), which follows the truth data. The predicted phase (dashed blue line) resolves the integer k_p to accomplish the unwrapping. Also shown is the envelope timing (gray line), used to unwrap the phase across fades. (d) Similar to (c) but illustrating phase continuity over a complicated fade sequence. (An overall slope of 40 rad/s was removed for display purposes.)

Figure 3 shows the phase noise PSD for $\delta\varphi(t) - \delta\varphi_{\text{truth}}(t)$ of Fig. 2(b), and compares this PSD to previous OTWTFT using the envelope only [i.e., finding $\delta\tau$ from Eq. (3) only].
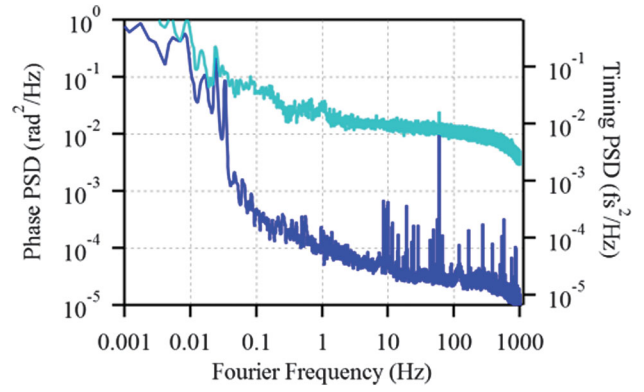
FIG. 3. Phase noise power spectral density of $\delta\varphi(t) - \delta\varphi_{\text{truth}}(t)$ (dark blue) in rad^2/Hz (left axis) and converted to fs^2/Hz (right axis). For comparison, the corresponding power spectral density extracted from the envelope pulse timing alone is also shown (light blue).

Above 1 Hz, the carrier-phase data is >25 dB lower, with a floor of $\sim 3 \times 10^{-5}$ rad^2/Hz ($\sim$20 as^2/Hz). Below 40 mHz, the two PSDs converge as the noise is limited by flicker ($1/f$) noise from variations in the delays within the transceivers.

Figure 4 shows the modified Allan deviation, σ_{MA}, from $\delta\varphi(t) - \delta\varphi_{\text{truth}}(t)$ at both 1% fades [e.g., Fig. 2(b)] and 26% fades. At 1% fades, the carrier-phase OTWTFT instability is $1.2 \times 10^{-17} t_{\text{av}}^{3/2}$ from 0.01 s to a few seconds. It then flattens from a few seconds to 10 s likely due to fluctuations in the transceiver delays from air-conditioning cycling, before dropping to 6×10^{-20} at 850 s. At short times, the carrier-phase OTWTFT is 10 times lower than for the envelope-only
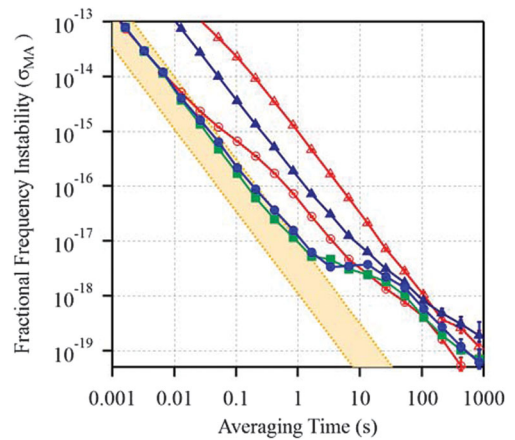
FIG. 4. Residual fractional frequency instability, σ_{MA}, for carrier-phase OTWTFT over a 4-km link with 1% fades (blue circles) and 26% fades (open red circles) compared to the corresponding envelope-only OTWTFT for 1% fades (blue triangles) and 26% fades (open red triangle). The carrier-phase OTWTFT instability over a shorted (0 km) link is also shown (green squares). Finally, the fundamental limit set by the time dependence of the atmospheric turbulence is indicated by the shaded orange box (at 10%–90% likelihood).

approach of previous OTWTFT. At the higher fade rate of 26%, the carrier-phase OTWTFT rises to 5.6×10^{-17} at 1 s and the envelope-only OTWTFT is 20 times higher still.

The measured instability of $\sim 10^{-17}$ at 1 s translates to a time deviation of 7 as, or equivalently 9 mrad, at 1 s, indicating reciprocity for a single-mode link holds to a remarkable degree even across a turbulent atmosphere. Nevertheless, there is a slight discrepancy between the open-path instability of 1.2×10^{-17} and shorted (no open-path) instability of 0.95×10^{-17}; see Fig. 4. We attribute this discrepancy to a slight breakdown in reciprocity from asynchronous sampling and time-dependent turbulence, i.e., exactly the additional term $\propto 0.5(t_{p,A} - t_{p,B})dT_{\text{link}}/dt$ discussed after Eq. (5). (Other effects that limit reciprocity [30,31,53] are unobserved in this configuration.) The time-dependent atmospheric piston phase noise, i.e., $T_{\text{link}}(t)$, is characterized by a spectral noise density of $af^{-7/3}$ [24,54] where f is the Fourier frequency and $a \sim 10^{-28}$ s^2 Hz$^{4/3}$. Approximating this PSD as $\sim f^{-2}$ gives a contribution to σ_{MA} of

$$\sigma_{\text{atm}}(t_{\text{av}}) = \pi\sqrt{3a/2}|t_{p,A} - t_{p,B}|t_{\text{av}}^{-3/2}. \qquad (6)$$

The asynchronous sampling, $|t_{p,A} - t_{p,B}|$, ranges from 0 to $(2\Delta f_r)^{-1} \sim 200$ μs; the shaded region in Fig. 4 shows $\sigma_{\text{atm}}(t_{\text{av}})$ for a 10%–90% range (20 μs $< |t_{p,A} - t_{p,B}| <$ 180 μs). The quadrature sum of the shorted σ_{MA} and $\sigma_{\text{atm}}(t_{\text{av}})$ at $|t_{p,A} - t_{p,B}| = 100$ μs agrees with the measured open-path results of 1.2×10^{-17} at 1 s.

The 4-km link distance demonstrated here is not the maximum range limit. Indeed, carrier-phase OTWTFT poses no additional constraints on range, excepting that the power-aperture product must be increased along with the link distance to maintain sufficient received comb power, comparable to the power requirements for coherent communications. At link distances >60 km, the time of flight reaches $(2\Delta f_r)^{-1}$ and the time stamps must be properly aligned to avoid an increase in the asynchronous sampling noise floor given by Eq. (6).

We have demonstrated phase comparisons between optical oscillators or clocks using the carrier phase of frequency comb pulses over turbulent free-space paths. Carrier-phase OTWTFT reaches 1.2×10^{-17} fractional stability at 1 s averaging time, corresponding to a time deviation of 7 as, despite the presence of turbulence-induced fades. In so doing, it connects the optical phases as distant sites and should enable correlated spectroscopy of distant optical clocks.

[1] F. Riehle, Optical clock networks, Nat. Photonics **11**, 25 (2017).

[2] T. Takano, M. Takamoto, I. Ushijima, N. Ohmae, T. Akatsuka, A. Yamaguchi, Y. Kuroishi, H. Munekane, B. Miyahara, and H. Katori, Geopotential measurements with synchronously linked optical lattice clocks, Nat. Photonics **10**, 662 (2016).

[3] B. Altschul et al., Quantum tests of the Einstein Equivalence Principle with the STE–QUEST space mission, Adv. Space Res. **55**, 501 (2015).

[4] C. Guerlin, P. Delva, and P. Wolf, Some fundamental physics experiments using atomic clocks and sensors, C.R. Phys. **16**, 565 (2015).

[5] R. Bondarescu, M. Bondarescu, G. Hetényi, L. Boschi, P. Jetzer, and J. Balakrishna, Geophysical applicability of atomic clocks: direct continental geoid mapping, Geophys. J. Int. **191**, 78 (2012).

[6] C. W. Chou, D. B. Hume, T. Rosenband, and D. J. Wineland, Optical clocks and relativity, Science **329**, 1630 (2010).

[7] P. Delva et al., Test of Special Relativity Using a Fiber Network of Optical Clocks, Phys. Rev. Lett. **118**, 221102 (2017).

[8] J. Müller, D. Dirkx, S. M. Kopeikin, G. Lion, I. Panet, G. Petit, and P. N. A. M. Visser, High performance clocks and gravity field determination, arXiv:1702.06761.

[9] A. Derevianko, Detecting dark matter waves with precision measurement tools, arXiv:1605.09717.

[10] A. Derevianko and M. Pospelov, Hunting for topological dark matter with atomic clocks, Nat. Phys. **10**, 933 (2014).

[11] P. Gill, When should we change the definition of the second?, Phil. Trans. R. Soc. A **369**, 4109 (2011).

[12] P. Delva and J. Lodewyck, Atomic clocks: new prospects in metrology and geodesy, Acta. Futura **7**, 67 (2013).

[13] P. Wolf et al., Quantum physics exploring gravity in the outer solar system: the SAGAS project, Exp. Astron. **23**, 651 (2009).

[14] P. Wcislo, P. Morzynski, M. Bober, A. Cygan, D. Lisak, R. Ciurylo, and M. Zawada, Searching for dark matter with optical atomic clocks, arXiv:160505763.

[15] M. Takamoto et al., Frequency ratios of Sr, Yb, and Hg based optical lattice clocks and their applications, C.R. Phys. **16**, 489 (2015).

[16] A. D. Ludlow, M. M. Boyd, J. Ye, E. Peik, and P. O. Schmidt, Optical atomic clocks, Rev. Mod. Phys. **87**, 637 (2015).

[17] I. Ushijima, M. Takamoto, M. Das, T. Ohkubo, and H. Katori, Cryogenic optical lattice clocks, Nat. Photonics **9**, 185 (2015).

[18] M. Schioppo et al., Ultrastable optical clock with two cold-atom ensembles, Nat. Photonics **11**, 48 (2017).

[19] D. G. Matei et al., 1.5 μm Lasers with Sub-10 mHz Linewidth, Phys. Rev. Lett. **118**, 263202 (2017).

[20] C. Lisdat et al., A clock network for geodesy and fundamental science, Nat. Commun. **7**, 12443 (2016).

[21] M. Xin, K. Şafak, M. Y. Peng, A. Kalaydzhyan, W.-T. Wang, O. D. Mücke, and F. X. Kärtner, Attosecond precision multi-kilometer laser-microwave network, Light Sci. Appl. **6**, e16187 (2017).

[22] S. Droste, F. Ozimek, T. Udem, K. Predehl, T. W. Hänsch, H. Schnatz, G. Grosche, and R. Holzwarth,

Optical-Frequency Transfer over a Single-Span 1840 km Fiber Link, Phys. Rev. Lett. **111**, 110801 (2013).

[23] A. Bercy, F. Stefani, O. Lopez, C. Chardonnet, P.-E. Pottie, and A. Amy-Klein, Two-way optical frequency comparisons at $5 \times 10 - 21$ relative stability over 100-km telecommunication network fibers, Phys. Rev. A **90**, 061802 (2014).

[24] K. Djerroud, O. Acef, A. Clairon, P. Lemonde, C. N. Man, E. Samain, and P. Wolf, Coherent optical link through the turbulent atmosphere, Opt. Lett. **35**, 1479 (2010).

[25] E. Samain, P. Vrancken, P. Guillemot, P. Fridelance, and P. Exertier, Time transfer by laser link (T2L2): characterization and calibration of the flight instrument, Metrologia **51**, 503 (2014).

[26] P. Laurent, D. Massonnet, L. Cacciapuoti, and C. Salomon, The ACES/PHARAO space mission, C.R. Phys. **16**, 540 (2015).

[27] P. Berceau and L. Hollberg, Laser time-transfer and space-time reference in orbit, *Proceedings of the Sixth Meeting on CPT and Lorentz Symmetry* (World Scientific, Bloomington, USA, 2013), pp. 220–223.

[28] J. Conklin, N. Barnwell, L. Caro, M. Carrascilla, O. Formoso, S. Nydam, P. Serra, and N. Fitz-Coy, Optical time transfer for future disaggregated small satellite navigation systems, in *AIAA/USU Conference on Small Satellite* (Digital Commons, Utah State University, UT, 2014).

[29] F. R. Giorgetta, W. C. Swann, L. C. Sinclair, E. Baumann, I. Coddington, and N. R. Newbury, Optical two-way time and frequency transfer over free space, Nat. Photonics **7**, 434 (2013).

[30] A. Belmonte, M. T. Taylor, L. Hollberg, and J. M. Kahn, Impact of atmospheric anisoplanaticity on earth-to-satellite time transfer over laser communication links, in *Proceedings Volume 10096, Free-Space Laser Communication and Atmospheric Propagation XXIX* (International Society for Optics and Photonics, San Francisco, CA, 2017), p. 1009605.

[31] C. Robert, J.-M. Conan, and P. Wolf, Impact of turbulence on high-precision ground-satellite frequency transfer with two-way coherent optical links, Phys. Rev. A **93**, 033860 (2016).

[32] J.-D. Deschênes, L. C. Sinclair, F. R. Giorgetta, W. C. Swann, E. Baumann, H. Bergeron, M. Cermak, I. Coddington, and N. R. Newbury, Synchronization of Distant Optical Clocks at the Femtosecond Level, Phys. Rev. X **6**, 021016 (2016).

[33] H. Bergeron, L. C. Sinclair, W. C. Swann, C. W. Nelson, J.-D. Deschênes, E. Baumann, F. R. Giorgetta, I. Coddington, and N. R. Newbury, Tight real-time synchronization of a microwave clock to an optical clock across a turbulent air path, Optica **3**, 441 (2016).

[34] L. C. Sinclair *et al.*, Synchronization of clocks through 12 km of strongly turbulent air over a city, Appl. Phys. Lett. **109**, 151104 (2016).

[35] H. J. Kang, B. J. Chun, J. Yang, Y.-J. Kim, and S.-W. Kim, Comb-based Optical Frequency Transfer in Free Space, in *Conference on Lasers Electro-Optics 2017* (Optical Society of America, San Jose, CA, 2017), p. STh4L.5.

[36] J. H. Shapiro, Reciprocity of the Turbulent Atmosphere, J. Opt. Soc. Am. **61**, 492 (1971).

[37] M. Fujieda, D. Piester, T. Gotoh, J. Becker, M. Aida, and A. Bauch, Carrier-phase two-way satellite frequency transfer over a very long baseline, Metrologia **51**, 253 (2014).

[38] A. Bauch, Time and frequency comparisons using radio-frequency signals from satellites, C.R. Phys. **16**, 471 (2015).

[39] F. Nakagawa, J. Amagai, R. Tabuchi, Y. Takahashi, M. Nakamura, S. Tsuchiya, and S. Hama, Carrier-phase TWSTFT experiments using the ETS-VIII satellite, Metrologia **50**, 200 (2013).

[40] C. E. Calosso, E. Bertacco, D. Calonico, C. Clivati, G. A. Costanzo, M. Frittelli, F. Levi, A. Mura, and A. Godone, Frequency transfer via a two-way optical phase comparison on a multiplexed fiber network, Opt. Lett. **39**, 1177 (2014).

[41] Z. Jiang, A. Czubla, J. Nawrocki, W. Lewandowski, and E. F. Arias, Comparing a GPS time link calibration with an optical fibre self-calibration with 200 ps accuracy, Metrologia **52**, 384 (2015).

[42] W.-K. Lee, F. Stefani, A. Bercy, O. Lopez, A. Amy-Klein, and P.-E. Pottie, Hybrid fiber links for accurate optical frequency comparison, Appl. Phys. B **123**, 161 (2017).

[43] M. Takamoto, T. Takano, and H. Katori, Frequency comparison of optical lattice clocks beyond the Dick limit, Nat. Photonics **5**, 288 (2011).

[44] D. B. Hume and D. R. Leibrandt, Probing beyond the laser coherence time in optical clock comparisons, Phys. Rev. A **93**, 032138 (2016).

[45] C. W. Chou, D. B. Hume, M. J. Thorpe, D. J. Wineland, and T. Rosenband, Quantum Coherence between Two Atoms beyond Q = 10^{15}, Phys. Rev. Lett. **106**, 160801 (2011).

[46] M. Chwalla, K. Kim, T. Monz, P. Schindler, M. Riebe, C. F. Roos, and R. Blatt, Precision spectroscopy with two correlated atoms, Appl. Phys. B **89**, 483 (2007).

[47] D. R. Leibrandt, M. J. Thorpe, J. C. Bergquist, and T. Rosenband, Field-test of a robust, portable, frequency-stable laser, Opt. Express **19**, 10278 (2011).

[48] Q.-F. Chen, A. Nevsky, M. Cardace, S. Schiller, T. Legero, S. Häfner, A. Uhde, and U. Sterr, A compact, robust, and transportable ultra-stable laser with a fractional frequency instability of 1×10^{-15}, Rev. Sci. Instrum. **85**, 113107 (2014).

[49] D. Świerad *et al.*, Ultra-stable clock laser system development towards space applications, Sci. Rep. **6**, 33973 (2016).

[50] S. Vogt, C. Lisdat, T. Legero, U. Sterr, I. Ernsting, A. Nevsky, and S. Schiller, Demonstration of a transportable 1 Hz-linewidth laser, Appl. Phys. B **104**, 741 (2011).

[51] W. Swann, L. Sinclair, I. Khader, N. R. Newbury, H. Bergeron, and J.-D. Deschenes, Free-Space Terminals for Optical Two-Way Time-Frequency Transfer, *Conference on Lasers Electro-Optics 2017* (Optical Society of America, San Jose CA, 2017), p. STh4L.4.

[52] See Supplemental Material at http://link.aps.org/supplemental/10.1103/PhysRevLett.120.050801 for a detailed derivation of Eqs. (2)–(5), fade statistics, details on the Kalman filter phase extraction and implementation, and a table of experimental values.

[53] G. Petit and P. Wolf, Relativistic theory for picosecond time transfer in the vicinity of the Earth, Astron. Astrophys. **286**, 971 (1994).

[54] L. C. Sinclair, F. R. Giorgetta, W. C. Swann, E. Baumann, I. Coddington, and N. R. Newbury, Optical phase noise from atmospheric fluctuations and its impact on optical time-frequency transfer, Phys. Rev. A **89**, 023805 (2014).